WASP-190b: Tomographic discovery of a transiting hot Jupiter.

L. Y. Temple,[1] C. Hellier,[1] Y. Almleaky,[2,3] D.R. Anderson,[1] F. Bouchy,[4] D.J.A. Brown,[5,6] A. Burdanov,[7]
A. Collier Cameron,[8] L. Delrez,[9] M. Gillon,[7] E. Jehin,[7] M. Lendl,[10,4] P.F.L. Maxted,[1] C. Murray,[11]
L. D. Nielsen,[4] F. Pepe,[4] D. Pollacco,[5,6] D. Queloz,[11] D. Ségransan,[4] B. Smalley,[1] S. Thompson,[11]
A.H.M.J. Triaud,[12] O.D. Turner,[4,1] S. Udry,[4] and R.G. West[5]

[1]*Astrophysics Group, Keele University, Staffordshire, ST5 5BG, UK*
[2]*Space and Astronomy Department, Faculty of Science, King Abdulaziz University,*
21589 Jeddah, Saudi Arabia
[3]*King Abdullah Centre for Crescent Observations and Astronomy (KACCOA), Makkah Clock, Saudia Arabia*
[4]*Observatoire astronomique de l'Université de Genève*
51 ch. des Maillettes, 1290 Sauverny, Switzerland
[5]*Department of Physics, University of Warwick,*
Gibbet Hill Road, Coventry, CV4 7AL, UK
[6]*Centre for Exoplanets and Habitability, University of Warwick,*
Gibbet Hill Road, Coventry CV4 7AL, UK
[7]*Space sciences, Technologies and Astrophysics Research (STAR) Institute,*
Université de Liège, Allée du 6 Août 17, 4000 Liège, Belgium
[8]*SUPA, School of Physics and Astronomy, University of St. Andrews*
North Haugh, Fife, KY16 9SS, UK
[9]*Cavendish Laboratory, J J Thomson Avenue,*
Cambridge, CB3 0HE, UK
[10]*Space Research Institute, Austrian Academy of Sciences, Schmiedlstr. 6, 80 42, Graz, Austria*
[11]*Cavendish Laboratory, J J Thomson Avenue, Cambridge, CB3 0HE, UK*
[12]*School of Physics & Astronomy, University of Birmingham, Edgbaston, Birmingham, B15 2TT, UK*

ABSTRACT

We report the discovery of WASP-190b, an exoplanet on a 5.37-day orbit around a mildly-evolved F6 IV-V star with $V = 11.7$, $T_{\rm eff} = 6400 \pm 100$ K, $M_* = 1.35 \pm 0.05\,M_\odot$ and $R_* = 1.6 \pm 0.1\,R_\odot$. The planet has a radius of $R_{\rm P} = 1.15 \pm 0.09\,R_{\rm Jup}$ and a mass of $M_{\rm P} = 1.0 \pm 0.1\,M_{\rm Jup}$, making it a mildly inflated hot Jupiter. It is the first hot Jupiter confirmed via Doppler tomography with an orbital period > 5 days. The orbit is also marginally misaligned with respect to the stellar rotation, with $\lambda = 21 \pm 6°$ measured using Doppler tomography.

Keywords: planets and satellites: detection — planets and satellites: individual (WASP-190b) — stars: individual (WASP-190)

1. INTRODUCTION

The Rossiter–McLaughlin (RM) effect, a distortion of the line profiles of a star caused by an occulting body blocking part of the stellar face, was first detected for a transiting hot Jupiter by Queloz et al. (2000) in observations of HD 209458, whereby the distortion was

detected as a perturbation to radial velocity measurements. It has since been used extensively to measure the projected angle between the planet's orbit and the stellar rotation axis in many hot-Jupiter systems (e.g. Triaud 2017). The current alignment of a planetary orbit with respect to the stellar rotation is an indicator of the dynamical history of the planet, and can point to the formation mechanisms at play.

One can also plot the line profiles as a function of phase, looking for the Doppler shadow of the planet

Corresponding author: L. Y. Temple
l.y.temple@keele.ac.uk

as it moves across the line profiles. The detection of the Doppler tomographic signal of a candidate exoplanet can rule out transit mimics such as blended eclipsing binaries. This "tomographic" method was first used in the discovery of a planet for WASP-33b (Collier Cameron et al. 2010b). The tomographic technique is particularly useful for systems with hotter and fast-rotating stars, with fewer and broader spectral lines, which may give only less-accurate radial-velocity measurements and thus were previously paid less attention by transit and radial velocity surveys. Thus Doppler tomography has now been used in the discovery of hot Jupiters transiting hot stars, including KELT-20b (Lund et al. 2017), HAT-P-67b (Zhou et al. 2017), WASP-167b/KELT-13b (Temple et al. 2017), MASCARA-1b (Talens et al. 2017) and WASP-189b (Anderson et al. 2018).

Brown et al. (2017) compare tomographic and RM analyses of the same datasets for six WASP systems. They find that the tomographic method consistently gives better constraints on values for the projected stellar rotational velocity $v \sin i_\star$ and the sky-projected obliquity angle λ. Note that the tomographic analysis method uses the line profiles more directly, while an RM analysis in terms of radial-velocity measurements (RVs) needs one to translate the change in the line profiles owing to a planet shadow into a change in the overall radial velocity (e.g. Hirano et al. 2011; Boué et al. 2013).

The number of known exoplanets has grown to the point where population studies can draw significant and meaningful conclusions about their bulk properties and dynamical histories. For example, Schlaufman (2018) uses a sample of 146 systems comprised of a solar-like star and a giant planet, brown dwarf, or low-mass stellar companion, to place a mass-limit boundary between hot Jupiters and brown dwarfs which relies on their formation mechanism. It is not possible, however, to perform the same scale of population studies for hot Jupiters orbiting early-type stars, due to the relative lack of such objects discovered so far (resulting, at least partially, from selection biases in past transit and radial-velocity surveys).

Hot Jupiters orbiting hot stars are of interest due to the orbital and physical differences between them and hot Jupiters orbiting later-type stars. They are more likely to be in misaligned orbits Winn et al. (2010); Triaud (2017), often have stars which rotate more quickly than the planet's orbit (e.g. Crouzet et al. 2017; Temple et al. 2017), and are inflated, with hotter dayside temperatures, due to the increased irradiation from their host star (Hartman et al. 2016; Temple et al. 2018). The increased irradiation might also result in

Table 1. Observations of WASP-190b.

Telescope/Instrument	Date	Notes
WASP-South	2006–2011	30137 pts.
TRAPPIST-South	2014 Nov 26	$I+z$, 7s exp.
SPECULOOS-Europa	2017 Oct 13	$I+z$, 10s exp.
CORALIE	2014 Aug–Oct	5 RVs
HARPS	2017 Oct 13	28 spectra taken including a transit
HARPS	2018 Oct	5 RVs

planetary magnetic fields which are stronger than in cooler Jupiters, since the continuous injection of energy into the interior of a gas giant might produce a more efficient planetary dynamo (Yadav & Thorngren 2017).

In this work, we report the discovery and characterisation of WASP-190b, a hot Jupiter orbiting a star of $T_{\rm eff} = 6400\,{\rm K}$ which can be found in *TESS* Sector 2 as TIC ID:116156517 (Ricker et al. 2015; Stassun et al. 2018). We use both tomographic and RM analyses to determine the geometry of the system, and confirm the existence of the planet via the detection of its Doppler shadow and by measuring its mass using orbital RV measurements.

2. DATA AND OBSERVATIONS

We observed WASP-190 using the WASP-South telescope (Hellier et al. 2011) at the South African Astronomical Observatory (SAAO) from 2006 to 2011. After the detection of a planet-like transit dip in the WASP lightcurve we confirmed the transit with a follow-up lightcurve obtained using the TRAPPIST-South telescope (Jehin et al. 2011), and proceeded to obtain reconnaissance spectroscopy with the Euler/CORALIE spectrograph (Queloz et al. 2001). These were sufficient to rule out a stellar-mass binary, but with relatively large errors were consistent with no motion at the level of $250\,{\rm m\,s^{-1}}$ and were inconclusive about whether the transiting body was a planet.

We thus attempted tomography of a transit, obtaining a series of 28 spectra through transit on the night of 2017 October 13 using the ESO 3.6-m/HARPS spectrograph (Pepe et al. 2002), accompanied by simultaneous photometry using the SPECULOOS-Europa telescope (Burdanov et al. 2018; Gillon 2018; Delrez et al. 2018). After tomographic detection of a planet-like signal, we obtained 5 further orbital RVs with HARPS to constrain the planetary mass.

The HARPS spectra were cross-correlated over a window of $\pm 350\,{\rm km\,s^{-1}}$, using a mask matching a G2 spectral type, and the standard HARPS Data Reduction Software as described by Baranne et al.

Table 2. RV measurements of WASP-190, taken using the CORALIE and HARPS spectrographs for this work.

BJD$_{TDB}$ −2,450,000	RV (km s^{-1})	σ_{RV} (km s^{-1})	BS (km s^{-1})	σ_{BS} (km s^{-1})
CORALIE (out of transit):				
6871.794771	0.89	0.05	−0.07	0.10
6895.811527	0.94	0.05	−0.16	0.10
6922.731329	0.90	0.03	−0.05	0.06
6952.511870	0.95	0.04	0.15	0.08
7000.625106	0.87	0.04	−0.22	0.08
8392.595422	0.84	0.07	−0.24	0.14
HARPS (including a transit):				
8040.529251	0.84	0.02	0.04	0.04
8040.540026	0.82	0.02	−0.04	0.04
8040.550489	0.84	0.02	0.05	0.04
8040.561472	0.86	0.02	−0.02	0.04
8040.572351	0.85	0.02	−0.05	0.04
8040.582918	0.85	0.02	−0.02	0.04
8040.593797	0.87	0.02	−0.00	0.04
8040.604572	0.92	0.02	0.02	0.04
8040.615243	0.89	0.02	−0.07	0.04
8040.626122	0.90	0.02	−0.13	0.04
8040.636897	0.87	0.02	−0.06	0.04
8040.647776	0.84	0.02	−0.01	0.04
8040.658459	0.80	0.02	−0.02	0.04
8040.669130	0.79	0.02	0.04	0.04
8040.680113	0.80	0.02	0.10	0.04
8040.690784	0.80	0.02	0.03	0.04
8040.701350	0.78	0.02	−0.07	0.04
8040.712334	0.76	0.02	−0.03	0.04
8040.723016	0.73	0.02	−0.03	0.04
8040.733791	0.76	0.02	−0.05	0.04
8040.744670	0.73	0.03	−0.05	0.06
8040.755341	0.76	0.03	0.05	0.06
8040.766220	0.77	0.03	0.09	0.06
8040.777100	0.81	0.03	−0.10	0.06
8040.787770	0.83	0.03	−0.02	0.06
8040.798545	0.82	0.03	0.10	0.06
8040.809112	0.85	0.03	−0.06	0.06
8040.820107	0.82	0.03	0.06	0.06
HARPS (out of transit):				
8393.843700	0.92	0.01	−0.20	0.02
8396.706300	0.73	0.01	0.10	0.02
8397.590800	0.86	0.04	−0.15	0.08
8398.611000	0.92	0.02	−0.24	0.04
8399.542350	0.85	0.04	−0.13	0.08

(1996), Pepe et al. (2002). We then analysed the cross-correlation functions (CCFs) themselves, and computed radial velocity (RV) measurements from the CCFs which we list in Table 2 along with bisector spans (BS).

We used the WASP photometric data to look for any evidence of rotational modulation of the host star, using the methods of Maxted et al. (2011). We find no such variability at periods longer than a day, with a 95%-confidence upper limit on the amplitude of 1 mmag.

3. STELLAR PARAMETERS FROM SPECTRAL ANALYSIS

In order to determine stellar parameters of WASP-190 we co-added the HARPS spectra obtained on the night of 2017 Oct 13 and performed a spectral analysis. We adopted a microturbulent velocity of $v_{mic} = 1.6 \, \mathrm{km \, s^{-1}}$ from the calibration of Bruntt et al. (2010) and a macro-turbulent velocity of $v_{mac} = 6.5 \, \mathrm{km \, s^{-1}}$ from the calibration of Doyle et al. (2014). We used the Hα line to determine an effective temperature $T_{eff} = 6400 \pm 100 \, \mathrm{K}$, while using the Na D feature to measure $\log g_* = 3.9 \pm 0.1$. We also determined the projected stellar rotational velocity $v \sin i_\star = 13.8 \pm 0.7 \, \mathrm{km \, s^{-1}}$, and the surface metallicity [Fe/H] $= -0.02 \pm 0.05$. These results are also listed in Table 3. Using the MKCLASS program (Gray & Corbally 2014) we then obtained a spectral type of F6 IV–V.

4. COMBINED MCMC ANALYSIS

We conduct an analysis very similar to that conducted by Temple et al. (2018) for WASP-174b, which involves the use of Markov Chain Monte Carlo (MCMC) methods to analyse the combined photometric and spectroscopic datasets. As one approach we use the in-transit spectroscopy data in the form of RV measurements, following the method of Hirano et al. (2011), and as a second approach we use the same data in the form of CCFs, following methods similar to that used by Brown et al. (2017); Temple et al. (2017). We call the former the Rossiter–McLaughlin (RM) analysis and the latter the tomographic analysis.

The code we use is described by Collier Cameron et al. (2007) and Pollacco et al. (2008), which in the latest version includes the tomographic analysis as described by Collier Cameron et al. (2010a). In both analyses, fitting the photometric lightcurves allows direct measurement of the planet-to-star area ratio $(R_p/R_\star)^2$, the impact parameter b and the key transit timing information T_c, P, T_{14} and by extension T_{12}, which are respectively the epoch of mid-transit, the orbital period, the transit duration and the duration of ingress (or equivalently egress). We use the value of T_{eff} obtained in the spectral analysis (see discussion in Section 7) as the starting

Table 3. All system parameters obtained in the combined analyses for WASP-190b .

1SWASP J003050.23–403424.3	
2MASS 00305023–4034243	
TIC ID:116156517	
Gaia DR2 4994237247949280000	
RA = $00^h30^m50.233^s$, Dec = $-40°34'24.36''$ (J2000)	
$V = 11.7 \pm 0.1$ (TYCHO2)	
Gaia DR2 Proper Motions:	
(RA) 38.23 ± 0.03 (Dec) -9.14 ± 0.04 mas/yr	
Gaia DR2 Parallax: 1.82 ± 0.03 mas	
Rotational Modulations: < 1 mmag (95%)	

Stellar parameters from spectral analysis:

Parameter (Unit)	Value
Spectral type	F6 IV–V
$T_{\rm eff}$ (K)	6400 ± 100
$\log g_*$	3.9 ± 0.1
[Fe/H]	-0.02 ± 0.05
$v \sin i_*$ (km s^{-1})	13.8 ± 0.7
$v_{\rm mic}$ (km s^{-1})	1.6 (assumed)
$v_{\rm mac}$ (km s^{-1})	6.5 (assumed)

Parameters from photometric and RV analysis:

Parameter (Unit)	DT Value (adopted):
P (d)	5.367753 ± 0.000004
T_c (BJD$_{\rm TDB}$)	2457799.1256 ± 0.0007
T_{14} (d)	0.186 ± 0.002
$T_{12} = T_{34}$ (d)	0.017 ± 0.002
$R_{\rm P}^2/R_*^2$	0.0062 ± 0.0002
b	0.45 ± 0.09
i (°)	87.1 ± 0.7
a (AU)	0.0663 ± 0.0008
M_* ($M_\odot$)	1.35 ± 0.05
R_* ($R_\odot$)	1.6 ± 0.1
$\log g_*$ (cgs)	4.17 ± 0.04
ρ_* ($\rho_\odot$)	0.34 ± 0.05
$T_{\rm eff}$ (K)	6400 ± 100
[Fe/H]	-0.02 ± 0.05
K (km s^{-1})	0.099 ± 0.009
$M_{\rm P}$ ($M_{\rm Jup}$)	1.0 ± 0.1
$R_{\rm P}$ ($R_{\rm Jup}$)	1.15 ± 0.09
$\log g_{\rm P}$ (cgs)	3.2 ± 0.1
$T_{\rm eql}$ (K)	1500 ± 50

Parameters from RM and DT analyses:

Parameter (Unit)	DT Value (adopted):	RM Value:
γ (km s^{-1})	0.82 ± 0.01	0.823 ± 0.009
λ (°)	21 ± 6	23 ± 12
$v_{\rm FWHM}$ (km s^{-1})	10 ± 1	–
$v \sin i_\star$ (km s^{-1})	13.3 ± 0.6	14.1 ± 0.7
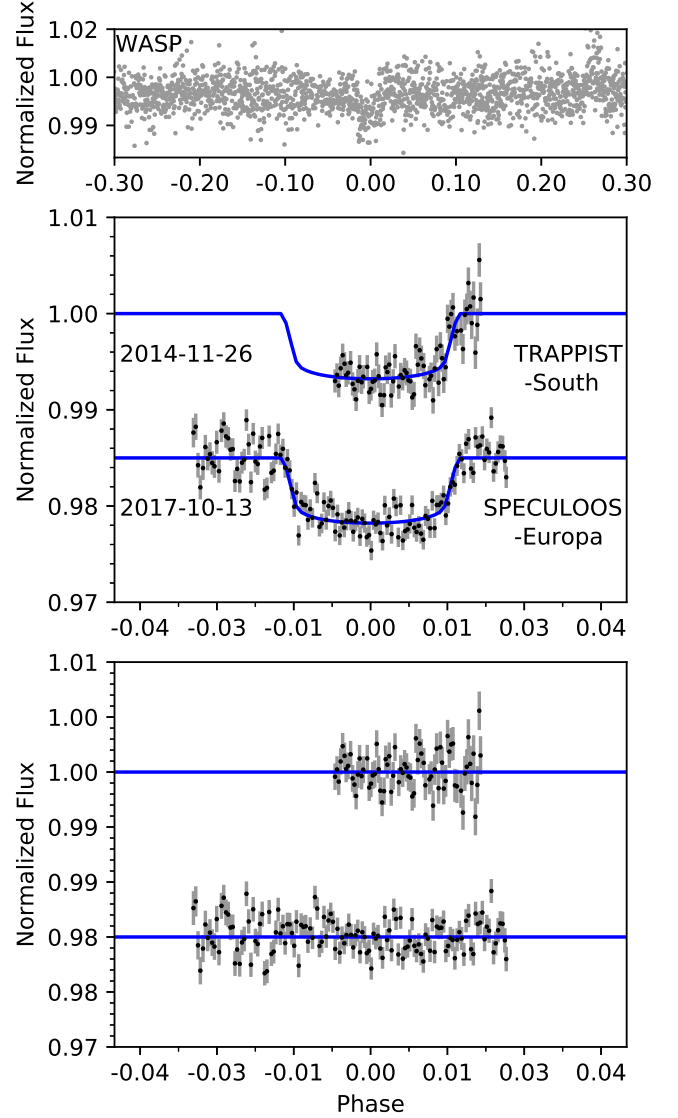
Figure 1. Top: the discovery lightcurve for WASP-190b (WASP-South). Middle: the two follow-up lightcurves with the best-fitting model shown in blue. Bottom: the residuals of the fits to the follow-up lightcurves.

value for the MCMC chains, and for each new value of $T_{\rm eff}$ we interpolate four-parameter law limb-darkening coefficients from the tables of Claret (2000, 2004). Stellar mass is calculated at each step using the Enoch–Torres relation (Enoch et al. 2010; Torres et al. 2010). The photometric data are displayed in Fig. 1 along with the best-fit model and residuals of the fit.

The RV analysis then enables measurement of the barycentric system velocity γ and the stellar reflex velocity semi-amplitude K. We expect that most hot Jupiters will settle into a circular orbit on a shorter timescale than their lifetimes (Pont et al. 2011), but

Table 4. Parameters for WASP-190 from BAGEMASS:

Parameter (Unit)	Value
Age (Gyr)	2.8 ± 0.4
M_* ($M_\odot$)	1.30 ± 0.05
$[\text{Fe/H}]_{\text{init}}$	0.03 ± 0.04

with an orbital period of ~ 5 days WASP-190b is entering the regime where eccentricity may remain. However, we do not have sufficient orbital RVs to constrain the eccentricity and so assume a circular orbit. We do not include the CORALIE measurements in the model adopted here, although including them changes the planetary mass by much less than the error bar.

Both the RM analysis and the tomographic analysis can allow the measurement of $v \sin i_\star$ and λ, while providing an additional constraint on the values of γ and b. However, it can often be the case that for RM analysis a prior on $v \sin i_\star$ is required in order to obtain a well-constrained fit, and so we adopt the spectral $v \sin i_\star$ as a prior for both analyses. In the tomographic analysis we also fit the local line width v_{FWHM}, resulting from stellar turbulence and instrumental broadening, which influences the width of the planetary perturbation of the line profiles, and whose shape is assumed to be Gaussian.

We show all RV measurements used in this work, along with the best fitting RV and RM models in Fig. 3. We also display the tomographic data (the time series of CCFs with the average of the out-of-transit CCFs subtracted from all CCFs) in Fig. 4, along with the best-fit planet model and residuals. The best fit parameters are listed in Table 3. We adopt the solution to the tomographic analysis (see Section 6) and, to avoid duplicating parameters derived from the same data (which are consistent in any case), the only parameters for which we list values from both analyses are γ, $v \sin i_\star$ and λ.

5. RESULTS FOR THE STAR

We find WASP-190 to have a large radius of $R_* = 1.6 \pm 0.1 R_\odot$ and a density of $\rho_* = 0.34 \pm 0.05 \rho_\odot$. This implies that the star is beginning to evolve away from the main sequence, which would be consistent with the spectral type of F6 IV–V.

The effective temperature (T_{eff}) was also obtained using the Infrared Flux Method (IRFM Blackwell & Shallis 1977). The stellar spectral energy distribution (SED) was obtained using literature broad-band photometry from 2MASS (Skrutskie et al. 2006), APASS9 B, V, g', r' and i' (Henden et al. 2015), USNO-B1 R (Monet et al. 2003) and WISE (Cutri & et al. 2012). The photometry was converted to fluxes and the best-fitting Kurucz (1993) model flux distribution found
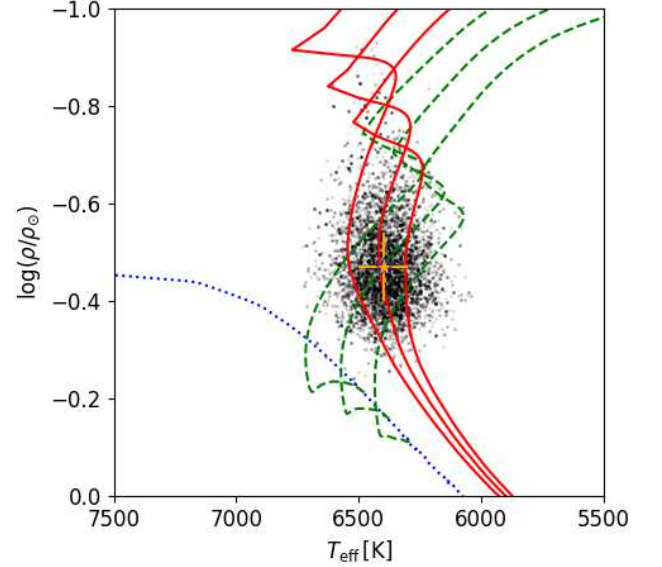

Figure 2. The best fitting evolutionary tracks and isochrones of WASP-190 obtained using BAGEMASS. Black points: individual realisations of the MCMC. Dotted blue line: Zero-Age Main Sequence (ZAMS) at best-fit [Fe/H]. Green dashed lines: evolutionary track for the best-fit [Fe/H] and mass, plus 1σ bounds. Red lines: isochrone for the best-fit [Fe/H] and age, plus 1σ bounds. Orange star: measured values of T_{eff} and ρ_* for WASP-190 obtained in the spectral and photometric analyses respectively.

and integrated to determine a bolometric flux of $5.27 \pm 0.26 \times 10^{-10}$ erg s^{-1} cm^{-2}. No visible interstellar lines were seen around the Na D line, so $E(B - V)$ was assumed to be zero. The IRFM was then used, with the 2MASS fluxes, to obtain a value of $T_{\text{eff}} = 6560 \pm 140$ K as well as an angular diameter of $\theta = 0.029 \pm 0.001$ mas. The *Gaia* DR2 (Gaia Collaboration et al. 2016, 2018) lists the parallax of WASP-190 as 1.82 ± 0.03 mas. Using these values and accounting for the correction to *Gaia* DR2 parallax values suggested by Stassun & Torres (2018), we obtain a stellar radius of $1.65 \pm 0.08 R_\odot$, which is consistent with our result from the MCMC analysis.

We investigate the age of WASP-190 using the open source software BAGEMASS[1] (Maxted et al. 2015). BAGEMASS allows the user to fit T_{eff} and M_* using stellar evolutionary models calculated for different He abundances and mixing lengths (GARSTEC; Weiss & Schlattl 2008). As inputs we use the values of T_{eff} and [Fe/H] derived from the spectral analysis in Section 3, and also use the value of ρ_* obtained in the combined analysis (Section 4) as a constraint.
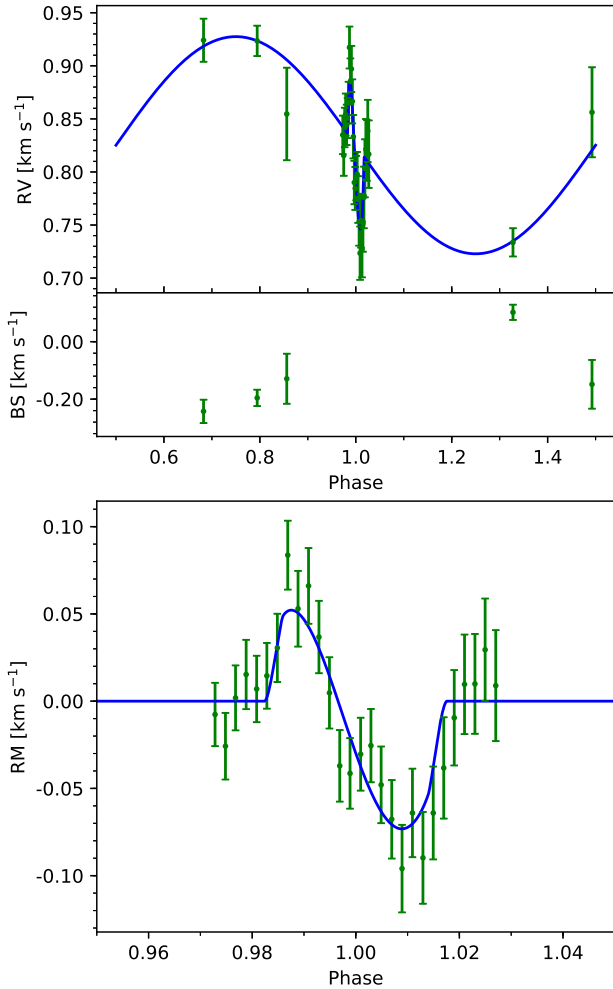
[1] http://sourceforge.net/projects/bagemass

Figure 3. Top: The HARPS RV measurements used in the analysis of WASP-190b. The blue line shows the best-fit Keplerian RV curve and the fit to the RM effect. Centre: the bisectors for the out-of-transit RVs plotted against phase, which show no correlation with the RV measurements. Bottom: The region around transit on a larger scale.

Assuming solar values for the He abundance and mixing length gave the best-fit solution. We display the corresponding isochrones and evolutionary tracks in Fig. 2. We find the current age of WASP-190 to be 2.8 ± 0.4 Gyr, implying that the star is beginning to evolve off the main sequence. This is consistent with our finding that the star has a radius larger than expected for a main sequence star. For comparison, the time taken to exhaust all hydrogen in the core is 3.8 ± 0.5 Gyr.

6. RESULTS FOR THE PLANET

We find a best fit K of $0.099 \pm 0.009 \, \mathrm{km \, s^{-1}}$, giving a planet mass of $M_p = 1.0 \pm 0.1 \, M_{\mathrm{Jup}}$. The fitted planetary radius is $1.15 \pm 0.09 \, \mathrm{R_{Jup}}$.

The in-transit RVs, showing the RM effect, are displayed in the lower panel of Fig. 3. The equivalent tomogram of the same data is shown in Fig. 4. Both are consistent with a planet in a prograde orbit. The projected spin-orbit angle, λ, is measured as $23 \pm 12°$ in the RM analysis and as $21 \pm 6°$ in the tomographic analysis. The planet trace is faint and hard to see, which we attribute to the star being relatively faint for tomographic analysis, at $V = 11.7$, and the transit dip being relatively shallow for a hot Jupiter, at 0.6%. The latter results from the star being relatively large at $1.6 \, \mathrm{R_{\odot}}$ when compared to the planet, which has only a mildly inflated radius of $1.15 \, \mathrm{R_{Jup}}$.

7. DISCUSSION AND CONCLUSIONS

We have shown that WASP-190b is a typical hot Jupiter with a mass of $1.0 \pm 0.1 \, M_{\mathrm{Jup}}$ and a mildly inflated radius of $1.15 \pm 0.09 \, R_{\mathrm{Jup}}$. It is in a 5.4-day orbit that is marginally misaligned with respect to the stellar rotation, with $\lambda = 21 \pm 6°$.

The measured values of $v \sin i_\star$ and λ are consistent between the spectral analysis, the tomographic analysis and the RM analysis. The tomographic analysis produced similar fits, giving a $v \sin i_\star$ value consistent with the spectroscopic value, regardless of whether we adopted the spectroscopic $v \sin i_\star$ as a prior. In contrast, the RM analysis was less constrained without a prior, and the fit tended to favour values that were too large. This often occurs for systems with a low impact parameter b, since it is difficult to differentiate the effects of $v \sin i_\star$ and λ on the shape of the RM curve when it is symmetrical (e.g. Albrecht et al. 2011). Since, in WASP-190, the impact parameter has a mid-level value of $b = 0.45$, this tendency should be reduced, but it may be that the low signal-to-noise of the data is leading the fit to be less constrained than usual. Overall, we found that the parameters were better constrained in the tomographic analysis than in the RM analysis, and so we adopt that fit.

While there is a well-established trend between the irradiation of a hot Jupiter and the inflation of its radius (e.g. Enoch et al. 2012), hot Jupiters also display a wide range of radii (e.g. Burrows et al. 2007). Sestovic et al. (2018) investigates the relationship between planet radius, mass and irradiation, finding that a more massive planet is usually less inflated than a low-mass planet of the same temperature, due to the planet's gravity counteracting the inflation. In Fig. 5 we show planetary radius as a function of equilibrium temperature, and use planetary mass as a third dimension, for all planets with $0.6 \, M_{\mathrm{Jup}} < M_p < 4.0 \, M_{\mathrm{Jup}}$ as listed in the TEP-Cat database (Southworth 2011). The figure indicates
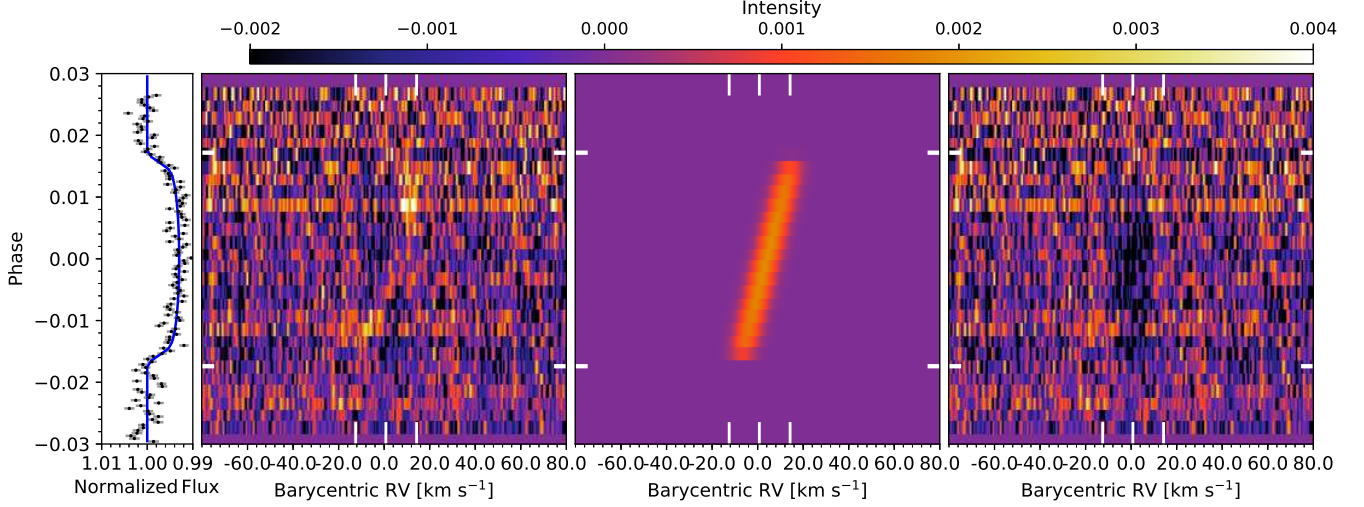
Figure 4. Centre-left: The Doppler tomogram comprised of the time series of residual HARPS CCFs calculated by subtracting the average of the out-of-transit CCFs from all CCFs. Left: the SPECULOOS-Europa lightcurve taken simultaneously with the HARPS observation. Centre-right: The best-fit planet model. Right: the residuals remaining after subtracting the best-fit planet model from the centre-left tomogram. In the three tomographic panels, the start and end times of the transit are marked with horizontal white dashes, while the vertical dashes mark respectively the positions of γ-$v \sin i_\star$, γ and γ+$v \sin i_\star$. We interpret the tomogram as showing a very faint, prograde planet signal which in places is completely masked by background noise.

that planets of a given mass and equilibrium temperature can have a wide range of radii, and shows that planets of $\sim 1\, M_{\rm Jup}$ like WASP-190b are not necessarily inflated, implying that the invocation of some third parameter is required. Possible causes of the disparity include different evolutionary histories, leading to different amounts of irradiation over time (e.g. Hartman et al. 2016), the possibility of internal heating mechanisms (e.g. Kurokawa & Inutsuka 2015; Ginzburg & Sari 2015; Thorngren & Fortney 2018; Ryu et al. 2018) and differences in the mass and metallicity of the planets' cores (e.g. Enoch et al. 2012).

With $\lambda = 21 \pm 6°$, WASP-190b is marginally misaligned. This is consistent with the known trend in hot-star systems, whereby planets around stars beyond the Kraft break have a wider range of obliquities, with most being in misaligned orbits (e.g. Winn et al. 2010; Dai & Winn 2017). The true orbit may be more strongly misaligned, however, since the value of $|\lambda|$ for non-polar misaligned orbits represents a lower limit for the true obliquity $|\psi|$. To measure ψ it would be necessary to independently measure the stellar equatorial rotational velocity v or stellar inclination $i_\star$ (for example, by looking for differential rotation effects as described by Cegla et al. 2016).
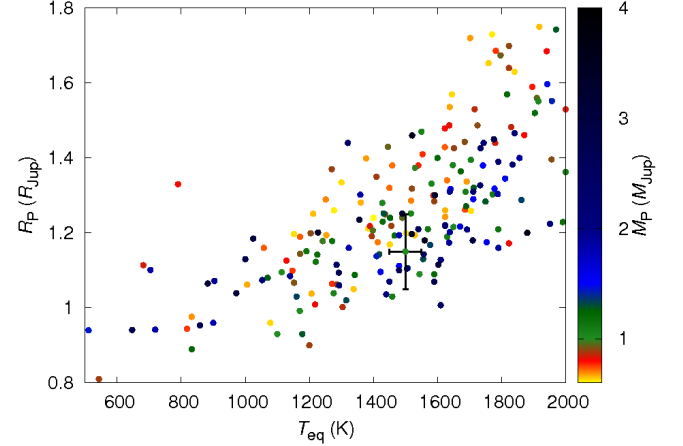
Figure 5. $R_{\rm p}$ vs. $T_{\rm eql}$, colour coded by mass, of all known planets with $0.6\, M_{\rm Jup} < M_{\rm p} < 4.0\, M_{\rm Jup}$. WASP-190b is displayed including the error bars on the measured radius and temperature.

Facilities: SuperWASP,ESO:3.6m(HARPS), Euler1.2m(CORALIE), WASP-South, TRAPPIST, SPECU-LOOS

Software: HARPS Data Reduction Software (Baranne et al. 1996; Pepe et al. 2002), BAGEMASS (Maxted et al. 2015), GARSTEC (Weiss & Schlattl 2008), MKCLASS (Gray & Corbally 2014)

REFERENCES

Albrecht, S., Winn, J. N., Johnson, J. A., et al. 2011, ApJ, 738, 50, doi: 10.1088/0004-637X/738/1/50

Anderson, D. R., Temple, L. Y., Nielsen, L. D., et al. 2018, ArXiv e-prints. https://arxiv.org/abs/1809.04897

Baranne, A., Queloz, D., Mayor, M., et al. 1996, A&AS, 119, 373

Blackwell, D. E., & Shallis, M. J. 1977, MNRAS, 180, 177, doi: 10.1093/mnras/180.2.177

Boué, G., Montalto, M., Boisse, I., Oshagh, M., & Santos, N. C. 2013, A&A, 550, A53, doi: 10.1051/0004-6361/201220146

Brown, D. J. A., Triaud, A. H. M. J., Doyle, A. P., et al. 2017, MNRAS, 464, 810, doi: 10.1093/mnras/stw2316

Bruntt, H., Bedding, T. R., Quirion, P.-O., et al. 2010, MNRAS, 405, 1907, doi: 10.1111/j.1365-2966.2010.16575.x

Burdanov, A., Delrez, L., Gillon, M., & Jehin, E. 2018, SPECULOOS Exoplanet Search and Its Prototype on TRAPPIST, ed. H. J. Deeg & J. A. Belmonte (Cham: Springer International Publishing), 1–17. https://doi.org/10.1007/978-3-319-30648-3_130-1

Burrows, A., Hubeny, I., Budaj, J., & Hubbard, W. B. 2007, ApJ, 661, 502, doi: 10.1086/514326

Cegla, H. M., Lovis, C., Bourrier, V., et al. 2016, A&A, 588, A127, doi: 10.1051/0004-6361/201527794

Claret, A. 2000, A&A, 363, 1081

—. 2004, A&A, 428, 1001, doi: 10.1051/0004-6361:20041673

Collier Cameron, A., Bruce, V. A., Miller, G. R. M., Triaud, A. H. M. J., & Queloz, D. 2010a, MNRAS, 403, 151, doi: 10.1111/j.1365-2966.2009.16131.x

Collier Cameron, A., Wilson, D. M., West, R. G., et al. 2007, MNRAS, 380, 1230, doi: 10.1111/j.1365-2966.2007.12195.x

Collier Cameron, A., Guenther, E., Smalley, B., et al. 2010b, MNRAS, 407, 507, doi: 10.1111/j.1365-2966.2010.16922.x

Crouzet, N., McCullough, P. R., Long, D., et al. 2017, AJ, 153, 94, doi: 10.3847/1538-3881/153/3/94

Cutri, R. M., & et al. 2012, VizieR Online Data Catalog, 2311

Dai, F., & Winn, J. N. 2017, AJ, 153, 205, doi: 10.3847/1538-3881/aa65d1

Delrez, L., Gillon, M., Queloz, D., et al. 2018, in Society of Photo-Optical Instrumentation Engineers (SPIE) Conference Series, Vol. 10700, Society of Photo-Optical Instrumentation Engineers (SPIE) Conference Series, 107001I

Doyle, A. P., Davies, G. R., Smalley, B., Chaplin, W. J., & Elsworth, Y. 2014, MNRAS, 444, 3592, doi: 10.1093/mnras/stu1692

Enoch, B., Collier Cameron, A., & Horne, K. 2012, A&A, 540, A99, doi: 10.1051/0004-6361/201117317

Enoch, B., Collier Cameron, A., Parley, N. R., & Hebb, L. 2010, A&A, 516, A33, doi: 10.1051/0004-6361/201014326

Gaia Collaboration, Prusti, T., de Bruijne, J. H. J., et al. 2016, A&A, 595, A1, doi: 10.1051/0004-6361/201629272

Gaia Collaboration, Brown, A. G. A., Vallenari, A., et al. 2018, A&A, 616, A1, doi: 10.1051/0004-6361/201833051

Gillon, M. 2018, Nature Astronomy, 2, 344, doi: 10.1038/s41550-018-0443-y

Ginzburg, S., & Sari, R. 2015, ApJ, 803, 111, doi: 10.1088/0004-637X/803/2/111

Gray, R. O., & Corbally, C. J. 2014, AJ, 147, 80, doi: 10.1088/0004-6256/147/4/80

Hartman, J. D., Bakos, G. Á., Bhatti, W., et al. 2016, AJ, 152, 182, doi: 10.3847/0004-6256/152/6/182

Hellier, C., Anderson, D. R., Collier Cameron, A., et al.
    2011, in European Physical Journal Web of Conferences,
    Vol. 11, European Physical Journal Web of Conferences,
    01004

Henden, A. A., Levine, S., Terrell, D., & Welch, D. L. 2015,
    in American Astronomical Society Meeting Abstracts,
    Vol. 225, American Astronomical Society Meeting
    Abstracts #225, 336.16

Hirano, T., Suto, Y., Winn, J. N., et al. 2011, ApJ, 742, 69,
    doi: 10.1088/0004-637X/742/2/69

Jehin, E., Gillon, M., Queloz, D., et al. 2011, The
    Messenger, 145, 2

Kurokawa, H., & Inutsuka, S.-i. 2015, ApJ, 815, 78,
    doi: 10.1088/0004-637X/815/1/78

Kurucz, R. 1993, ATLAS9 Stellar Atmosphere Programs
    and 2 km/s grid. Kurucz CD-ROM No. 13. Cambridge,
    Mass.: Smithsonian Astrophysical Observatory, 1993., 13

Lund, M. B., Rodriguez, J. E., Zhou, G., et al. 2017, AJ,
    154, 194, doi: 10.3847/1538-3881/aa8f95

Maxted, P. F. L., Serenelli, A. M., & Southworth, J. 2015,
    A&A, 575, A36, doi: 10.1051/0004-6361/201425331

Maxted, P. F. L., Anderson, D. R., Collier Cameron, A.,
    et al. 2011, PASP, 123, 547, doi: 10.1086/660007

Monet, D. G., Levine, S. E., Canzian, B., et al. 2003, AJ,
    125, 984, doi: 10.1086/345888

Pepe, F., Mayor, M., Rupprecht, G., et al. 2002, The
    Messenger, 110, 9

Pollacco, D., Skillen, I., Collier Cameron, A., et al. 2008,
    MNRAS, 385, 1576,
    doi: 10.1111/j.1365-2966.2008.12939.x

Pont, F., Husnoo, N., Mazeh, T., & Fabrycky, D. 2011,
    MNRAS, 414, 1278,
    doi: 10.1111/j.1365-2966.2011.18462.x

Queloz, D., Eggenberger, A., Mayor, M., et al. 2000, A&A,
    359, L13

Queloz, D., Mayor, M., Udry, S., et al. 2001, The
    Messenger, 105, 1

Ricker, G. R., Winn, J. N., Vanderspek, R., et al. 2015,
    Journal of Astronomical Telescopes, Instruments, and
    Systems, 1, 014003, doi: 10.1117/1.JATIS.1.1.014003

Ryu, T., Zingale, M., & Perna, R. 2018, MNRAS, 481,
    5517, doi: 10.1093/mnras/sty2638

Schlaufman, K. C. 2018, ApJ, 853, 37,
    doi: 10.3847/1538-4357/aa961c

Sestovic, M., Demory, B.-O., & Queloz, D. 2018, A&A, 616,
    A76, doi: 10.1051/0004-6361/201731454

Skrutskie, M. F., Cutri, R. M., Stiening, R., et al. 2006, AJ,
    131, 1163, doi: 10.1086/498708

Southworth, J. 2011, MNRAS, 417, 2166,
    doi: 10.1111/j.1365-2966.2011.19399.x

Stassun, K. G., & Torres, G. 2018, ApJ, 862, 61,
    doi: 10.3847/1538-4357/aacafc

Stassun, K. G., Oelkers, R. J., Pepper, J., et al. 2018, AJ,
    156, 102, doi: 10.3847/1538-3881/aad050

Talens, G. J. J., Albrecht, S., Spronck, J. F. P., et al. 2017,
    A&A, 606, A73, doi: 10.1051/0004-6361/201731282

Temple, L. Y., Hellier, C., Albrow, M. D., et al. 2017,
    MNRAS, 471, 2743, doi: 10.1093/mnras/stx1729

Temple, L. Y., Hellier, C., Almleaky, Y., et al. 2018,
    MNRAS, 480, 5307, doi: 10.1093/mnras/sty2197

Thorngren, D. P., & Fortney, J. J. 2018, AJ, 155, 214,
    doi: 10.3847/1538-3881/aaba13

Torres, G., Andersen, J., & Giménez, A. 2010, A&A Rv, 18,
    67, doi: 10.1007/s00159-009-0025-1

Triaud, A. H. M. J. 2017, The Rossiter–McLaughlin Effect
    in Exoplanet Research, ed. H. J. Deeg & J. A. Belmonte
    (Cham: Springer International Publishing), 1–27.
    https://doi.org/10.1007/978-3-319-30648-3_2-1

Weiss, A., & Schlattl, H. 2008, Ap&SS, 316, 99,
    doi: 10.1007/s10509-007-9606-5

Winn, J. N., Fabrycky, D., Albrecht, S., & Johnson, J. A.
    2010, ApJL, 718, L145,
    doi: 10.1088/2041-8205/718/2/L145

Yadav, R. K., & Thorngren, D. P. 2017, ApJL, 849, L12,
    doi: 10.3847/2041-8213/aa93fd

Zhou, G., Bakos, G. Á., Hartman, J. D., et al. 2017, AJ,
    153, 211, doi: 10.3847/1538-3881/aa674a